Materials Research Bulletin 48 (2013) 1352–1356

Contents lists available at SciVerse ScienceDirect

Materials Research Bulletin

journal homepage: www.elsevier.com/locate/matresbu

Ethylenediamine-assisted solvothermal synthesis of one-dimensional $Cd_xZn_{(1-x)}S$ solid solutions and their photocatalytic activity for nitrobenzene reduction

Hongwei Wei [a], Hechun Jiang [a], Zhen Zheng [b], Quanqin Zhao [a,*], Qingyin Wu [c,**], Jinhua Zhan [a]

[a] Key Laboratory of Colloid and Interface Chemistry, Ministry of Education, Department of Chemistry, Shandong University, Jinan 250100, Shandong, PR China
[b] School of Environment Science and Engineering, Shandong University, Jinan 250100, Shandong, PR China
[c] Department of Chemistry, Zhejiang University, Hangzhou 310027, Zhejiang, PR China

ARTICLE INFO

Article history:
Received 25 May 2012
Received in revised form 19 October 2012
Accepted 12 November 2012
Available online 27 December 2012

Keywords:
A. Semiconductors
B. Chemical synthesis
C. X-ray diffraction
D. Catalytic properties

ABSTRACT

A series of one-dimensional $Cd_xZn_{(1-x)}S$ semiconductor alloys were prepared via a hydrothermal method with the assistance of ethylenediamine at 180 °C for 12 h. The products were characterized by X-ray diffraction, scanning electron microscopy, transmission electron microscopy, nitrogen adsorption/desorption and Fourier transform infrared techniques. With the value of x increased, the band gap of $Cd_xZn_{(1-x)}S$ semiconductor alloys gradually decreased indicating that catalysts were exchanged to visible-light response. Photocatalytic reduction results showed that $Cd_{0.73}Zn_{0.27}S$ exhibited the highest photocatalytic activity toward photo production of aniline via nitrobenzene reduction under visible irradiation respectively. The reaction mechanism was also discussed.

1. Introduction

Semiconductor photocatalysis has aroused growing interests since photoinduced splitting of water on TiO_2 electrode was reported in 1972 [1]. For semiconductor photocatalysts, some disadvantages such as limited visible-light absorption, incomplete charge separation and little internal surface area, remain to be pivotal problems that hinder practical applications of this high efficient, "green" technique. General strategies such as the ion doping [2–8], coupling of two semiconductors [9–11], metal deposition [12], or surface chemical modification etc. [13–15] have involved to solve the above-mentioned problems. One-dimensional (1D) nanosized heterostructures, such as ZnO/ZnS [16], CdS/MoS_2 [17], ZnO/CdSe [18] heterostructures, are considered as excellent candidates because of their high surface areas, modulated band structures and promoted separation of photogenerated charge carriers. For photocatalytic reactions occuring on the materials' surface, the reactivity behavior is determined not only by the specific surface area or pore size distribution, but also the adsorbed surface functional groups [19].

$Cd_xZn_{(1-x)}S$ semiconductor alloys have attracted prime attention recently. Due to their tunable band structures, $Cd_xZn_{(1-x)}S$ semiconductor alloys are widely used in H_2 production [20,21], environmental cleaning [22,23] under visible-light. They are also promising materials in solar cells, photodetectors, diodes and optical recording [24]. $Cd_xZn_{(1-x)}S$ nanostructures, such as nanoparticles [25], nanoribbons [26], nanowires [27,28], nanocombs [29], and nanosheets [30], have been reported. However, the synthesis of 1D $Cd_xZn_{(1-x)}S$ nanostructures with highly crystalline properties via a precipitate-solvothermal approach has not been reported.

The photoinduced reduction of nitroarenes may be used as an alternative method for fine chemicals production. TiO_2 has been demonstrated as an appropriate candidate for aniline (AN) evaluation via nitrobenzene (NB) photoreduction [31–33]. In this study, we report the ethylenediamine (en)-assisted synthesis of hexagonal phased 1D $Cd_xZn_{(1-x)}S$ nanostructures. Photocatalytic production of AN via NB reduction was carried out under visible ($\lambda > 420$ nm) and UV-light in the presence of CH_3OH to evaluate their photocatalytic activity. Results showed that $Cd_{0.73}Zn_{0.27}S$ exhibited the highest photocatalytic activity under visible light respectively.

2. Experimental

2.1. Materials

All chemicals were of analytical grade and used as received without further purification. Zinc chloride powders ($ZnCl_2$) were purchased form Aladdin Reagent Co. Ltd. Copper chloride ($CuCl_2{\cdot}2H_2O$) and thiocarbamide were obtained from Sinopharm

* Corresponding author. Tel.: +86 531 8838 2378; fax: +86 531 8836 6280.
** Corresponding author. Tel.: +86 571 88914042; fax: +86 571 87951895.
E-mail addresses: zhaoqq@sdu.edu.cn (Q. Zhao), qywu@zju.edu.cn (Q. Wu).

0025-5408/$ – see front matter © 2013 Published by Elsevier Ltd.
http://dx.doi.org/10.1016/j.materresbull.2012.11.070

Chemical Reagent Co. Ltd. Ethylendiamine was purchased from Tianjin Dengke Chemical Reagent Co. Ltd. Cadmium chloride hydrate ($CdCl_2{\cdot}2.5H_2O$) was purchased from Shanghai Chemical Reagents Company.

2.2. Synthesis of $Cd_xZn_{(1-x)}S$ semiconductor alloys

$Cd_xZn_{(1-x)}S$ semiconductor alloys were prepared via a-pot solvothermal process. In a typical procedure, appropriate amount of $CdCl_2{\cdot}2.5H_2O$ and $ZnCl_2$ (2 mmol in total) and 4 mmol of $CS(NH_2)_2$ were ultrasonically dispersed in 40 ml mixed solvent of ethylenediamine and deionized water (volume ratio = 1:1). The resulted precursors were transferred into a 55 ml Teflon-lined stainless steel autoclave and kept at 180 °C for 12 h. After the autoclaves cooled to room temperature, yellow or white products were collected, washed with deionized water and dried in vacuum at 70 °C for 10 h. A series of $Cd_xZn_{(1-x)}S$ samples were obtained by controlling the added $CdCl_2{\cdot}2.5H_2O$ at 2, 1, 0.5, 0.2, and 0 mmol.

2.3. Characterization

Chemical composition analysis of $Cd_xZn_{(1-x)}S$ semiconductor alloys was determined by atomic absorption spectroscopy (AAS, HP3510). The X-ray powder diffraction (XRD) analysis was operated on an X-ray diffractometer (Bruker D8) with Cu Kα radiation (λ = 1.5418 Å) at the scanning rate of 2°/min for 2θ ranging from 20 to 80°, and the tube voltage and electric current were 40 kV and 20 mA respectively. UV–vis absorption spectrum was conducted by a TU-1901 UV–vis spectrophotometer. The morphology and structure were studied by transmission electron microscopy (TEM, JEM-1011, 100 kV), high-resolution TEM (HRTEM, JEM-2100, 200 kV), scanning electron microscopy (SEM, JSM-6700F) and electron diffraction spectrum (EDS) techniques. Fourier transform infrared (FT-IR) spectral were measured on a FT-IR spectrometer (VERTEX-70) from 4000 cm^{-1} to 400 cm^{-1} at room temperature. The Brunauer–Emmett–Teller (BET) specific surface area, Barrett–Joyner–Halenda pore size and distribution were determined by nitrogen (N_2) adsorption/desorption at 77 K using a QuadraSorb SI surface area analyzer after degassing the samples at 100 °C for 10 h.

2.4. Photocatalytic reduction of NB

Photocatalytic reduction of NB was carried out in an XPA-photochemical reactor (XuJiang Electromechanical Plant, Nanjing, China). For each photochemical reaction, $Cd_xZn_{(1-x)}S$ sample (50 mg) was ultrasonically dispersed in 10 ml NB-CH_3OH solution (1/99, v/v). Here, side-irradiation quartz cells were used as the reaction vessels. Ultrapure N_2 was bubbled through the cells for 3 h to eliminate dissolved oxygen before illumination, and the reaction system was magnetic stirred in the whole procedure. The illumination system was supplied by a 500 W Hg lamp. Optical cutoff filters were used to remove the light at wavelength below 420 nm. After irradiated for 42 h, the degradation products were detected using a gas chromatography (GC9790II, Fuli, Zhejiang), equipped a flame ion detector (FID) and a KB-1 capillary column (30 m × 0.32 mm × 0.25 μm).

3. Results and discussion

3.1. Characterization of $Cd_xZn_{(1-x)}S$ semiconductor alloys

X-ray diffraction (XRD) patterns of the synthesized $Cd_xZn_{(1-x)}S$ semiconductor alloys are shown in Fig. 1, together with the standard patterns of hexagonal CdS (JCPDS 36-1450) and ZnS (JCPDS 65-3414) shown at below for comparison. All the patterns present the similar profiles with a slight shift, indicating that the obtained products are not physical mixtures of CdS and ZnS phases but $Cd_xZn_{(1-x)}S$ semiconductor alloys. Owning to the larger radii of Cd^{2+} (0.97 Å) than that of Zn^{2+} (0.74 Å), the peaks are shifted to a lower-angel as the value of x increased [34]. Compared with the standard XRD cards, the unusually strong peak of (0 0 2) indicates the preferential orientation of [0 0 1] direction [35]. XRD analysis suggests that 1D hexagonal $Cd_xZn_{(1-x)}S$ semiconductor alloys were prepared in our study.

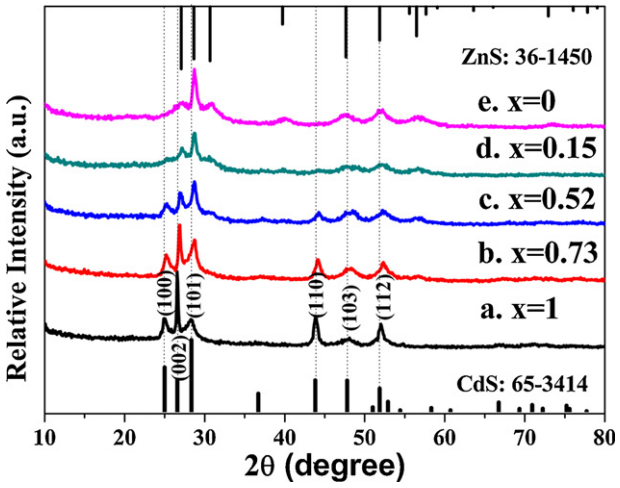

Fig. 1. XRD patterns of $Cd_xZn_{(1-x)}S$ semiconductor alloys with (a) x = 1, (b) x = 0.73, (c) x = 0.52, (d) x = 0.15, and (e) x = 0.

Atomic absorption spectroscopy (AAS) was used to investigate chemical compositions of $Cd_xZn_{(1-x)}S$ (x = 0–1) photocatalysts. Results showed that $Cd_xZn_{(1-x)}S$ semiconductor alloys with x = 1, 0.73, 0.52, 0.15, and 0 were prepared in our study. Compared with the initial added Cd^{2+}/Zn^{2+}, a decrease of Zn content is observed (Table 1), which is caused by the smaller solubility product constant (K_{sp}) for CdS than that of ZnS [36].

Fig. 2(a) gives UV–vis diffuse reflectance spectra (DRS) of the as-prepared $Cd_xZn_{(1-x)}S$ semiconductor alloys, together with colors of the corresponding samples (inset). As shown, the absorption edges are blue-shift with the increase of Zn content, which is in good agreement with the XRD results and the gradually lighted colors. Band gaps of the semiconductor alloys could be evaluated through the formula: $\alpha h\nu \propto (h\nu - E_g)^{n/2}$ [37], where α, $h\nu$, and E_g are the absorption coefficient, photon energy and band gap. The value of n is decided by whether the semiconductor is direct (n = 1) or indirect (n = 2) transition. Herein, the value of n is determined as 1 by roughly estimating from the absorption edge. Band gaps of 2.38 eV, 2.46 eV, 2.52 eV, 3.40 eV and 3.52 eV were given by the $(\alpha h\nu)^2 - h\nu$ curves (Fig. 2(b)) for the as-prepared $Cd_xZn_{(1-x)}S$ semiconductor alloys, which are comparable to the previous reports [38].

Table 1
Properties summary of $Cd_xZn_{(1-x)}S$ semiconductor alloys.

$Cd_xZn_{(1-x)}S$ samples	Initial Cd^{2+}/Zn^{2+} (molar ratio)	Chemical composition (x value)	Bandgap (eV)	Conduction band potential (V)	BET (m^2/g)
a	–[a]	1	2.38	−0.97	30.4
b	1:1	0.73	2.46	−0.88	58.9
c	1:3	0.52	2.52	−0.81	76.4
d	1:9	0.15	3.40	−1.46	120
e	0[b]	0	3.52	−1.48	140

[a] In the absence of Zn^{2+}.
[b] In the absence of Cd^{2+}.

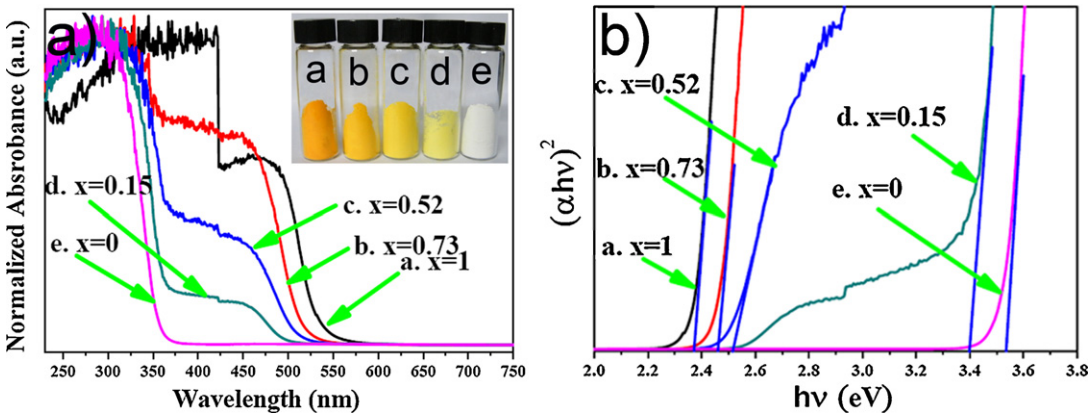

Fig. 2. (a) UV–vis diffuse reflectance spectral of $Cd_xZn_{(1-x)}S$ semiconductor alloys with x = 1, 0.73, 0.52, 0.15 and 0. Inset is the corresponding samples. (b) Band gap energy calculated by the extrapolating method.

Morphologic and structural analysis of $Cd_xZn_{(1-x)}S$ semiconductor alloys was carried out by SEM, TEM, HRTEM and EDS techniques, and the images were shown in Fig. 3 by taking $Cd_{0.73}Zn_{0.27}S$ as a typical example. The Fig. 3(a), representative SEM image of $Cd_{0.73}Zn_{0.27}S$ showed that the products were mainly composed of 1D nanostructure with large aggregation. As seen in the TEM image (Fig. 3(b)), the smooth, flexible, and almost transparent nanobelts are 20–50 nm in width and several micrometers in length with highly crystalline. The HRTEM image was given in Fig. 3(c). Clearly observed lattice fringes with d spacing of 0.33 nm corresponded to the (0 0 2) crystal planes, which was consistent with XRD results. EDS (Fig. 3(d)) analysis conducted on the central region of one $Cd_{0.73}Zn_{0.27}S$ nanobelt indicated the nanobelt was mainly composed of Cd, Zn, S elements with Cd/Zn/S ratio of 0.73:0.3:1.03 (a stoichiometry to $Cd_{0.73}Zn_{0.27}S$). With the increase of x, the morphology of $Cd_xZn_{(1-x)}S$ exchanged from nanorods to thin belt-like. As we all known, ethylenediamine is a common chelating ligand for coordination compounds for its two hydrophilic functional groups of $-NH_2$. Experiments also show that one-dimensional nanomaterials are easily formed in the presence of ethylenediamine [39–41].

N_2 adsorption/desorption investigations were carried out to study the textural properties of $Cd_xZn_{(1-x)}S$ semiconductor alloys. The adsorption/desorption isotherm (Fig. 4) of the representative $Cd_{0.73}Zn_{0.27}S$ sample show a type III isotherm with a clear H_3 hysteresis loop [42]. Barrett–Joyner–Helenda (BJH) analysis reveals the sample possesses an average pore diameter of

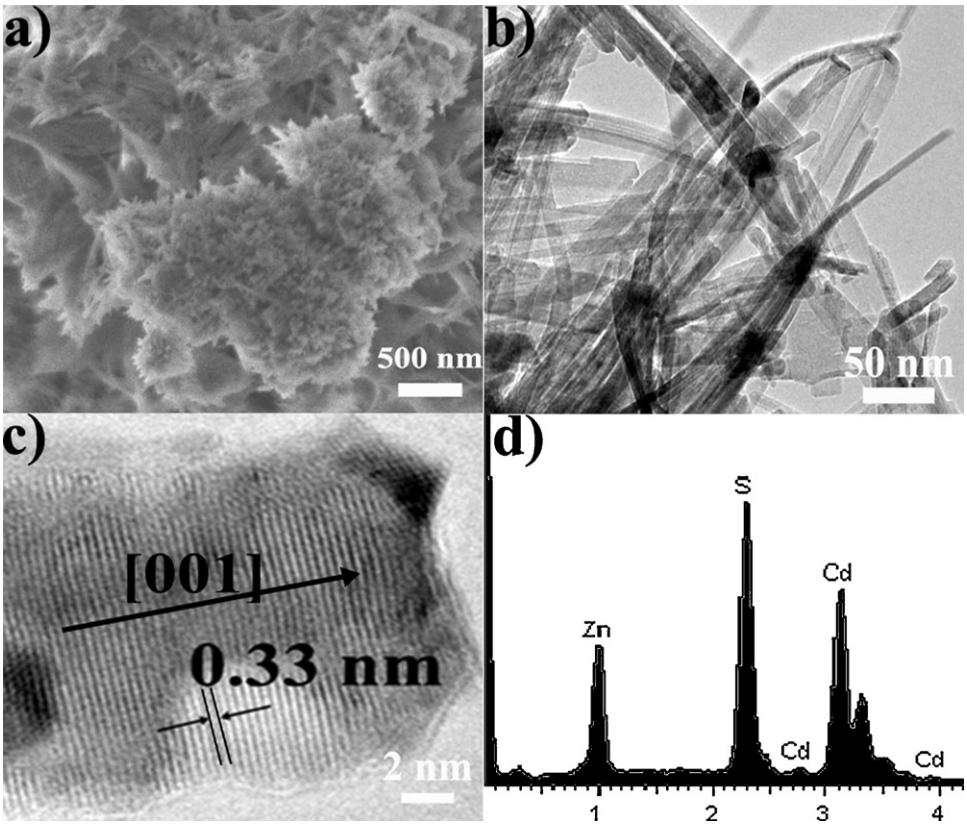

Fig. 3. SEM (a), TEM (b) HRTEM (c) images and EDS spectrum (d) of $Cd_{0.73}Zn_{0.27}S$ sample.

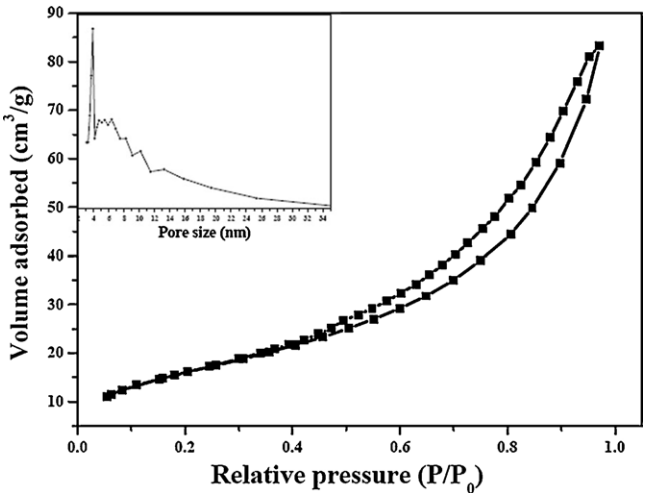

Fig. 4. N_2 adsorption/desorption isotherm and pore size distribution (inset) of $Cd_{0.73}Zn_{0.27}S$ sample.

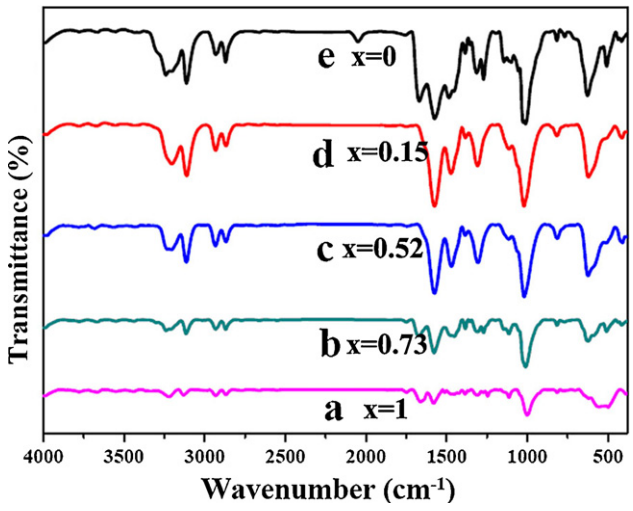

Fig. 5. FT-IR spectra of $Cd_xZn_{(1-x)}S$ semiconductor alloys with (a) $x = 1$, (b) $x = 0.73$, (c) $x = 0.52$, (d) $x = 0.15$, and (d) $x = 0$.

2–5 nm with the BET specific surface area of 58.9 m^2/g. The BET specific surface area increased with the increase of Zn content (Table 1.), which was caused by the disappearance of nanorods partly and the formation of thin belt-like nanostructures.

FT-IR spectra (Fig. 5) of $Cd_xZn_{(1-x)}S$ samples represent the similar absorption peaks with decreased intensity as x value increases. The broad peak at around 3240 cm^{-1} and the sharp peak at 1306 cm^{-1} were assigned to the stretching vibration and bending vibration of O–H due to the adsorbed –OH. The peaks at 624, 1019, 1460, 1580, 2940, 3105 cm^{-1} attributed to the absorption of $M(en)Cl_2$ (M = Cd, Zn), indicating the presence of en molecules on $Cd_xZn_{(1-x)}S$ samples' surface [43]. Adjacent cadmium ions and zinc ions are bridged through the transconformation of en molecule as reported [44]. The gradually increasing intensity is likely caused by the stronger complexation of Zn^{2+} and en molecules than that of Cd^{2+}, which can be confirmed further by the preferential formation $ZnS(en)_{0.5}$ and CdS [45–47] in pure en.

3.2. Photocatalytic activity

Photocatalytic activities of $Cd_xZn_{(1-x)}S$ semiconductor alloys were studied by the photocatalytic production of AN via NB reduction under visible and UV-light irradiation. Gas chromatogram (GC) results showed that the main products were nitrosobenzene and aniline. Photocatalytic nitrosobenzene and aniline evolution over different catalysts under visible and UV-light light irradiation were represented in Fig. 6. $Cd_{0.73}Zn_{0.27}S$ showed the highest activity for AN production under visible-light irradiation respectively. No nitrosobenzene or aniline was detected in the absence of only catalysts or light irradiation. The reason is discussed as follows.

It is well known that the narrow band gap, relative negative conduction band potential, efficient migration of charge carriers, and high BET specific surface are favorable for NB photocatalytic reduction [40]. For $Cd_xZn_{(1-x)}S$ semiconductor alloys, the conduction band potentials (E_{CB}) (vs. SCE, pH = 7) are shown in Table 1. The values were determined from Eqs. (1) and (2) as reported in Ref. [48]. There are two variables (x and E_g [$Cd_xZn_{(1-x)}S$]) in Eq. (3) while E_{VB}(CdS), E_{VB}(CdS) and E_{VB}(ZnS) are constant.

$$E_{VB}[Cd_xZn_{(1-x)}S] = xE_{VB}(CdS) + (1-x)E_{VB}(ZnS) \quad (1)$$

$$E_{CB}[Cd_xZn_{(1-x)}S] = E_{VB}[Cd_xZn_{(1-x)}S] - Eg[Cd_xZn_{(1-x)}S] \quad (2)$$

So,

$$E_{CB}[Cd_xZn_{(1-x)}S] = x(E_{VB}(CdS) - E_{VB}(CdS)) - Eg[Cd_xZn_{(1-x)}S] + E_{VB}(ZnS) \quad (3)$$

Although $Cd_{0.73}Zn_{0.27}S$ possesses a low surface area compared with other $Cd_xZn_{(1-x)}S$ samples, the narrow band gap would allow for more visible-light absorption and the generation of electron–hole pairs further. The thin nanobelts lead to reduced

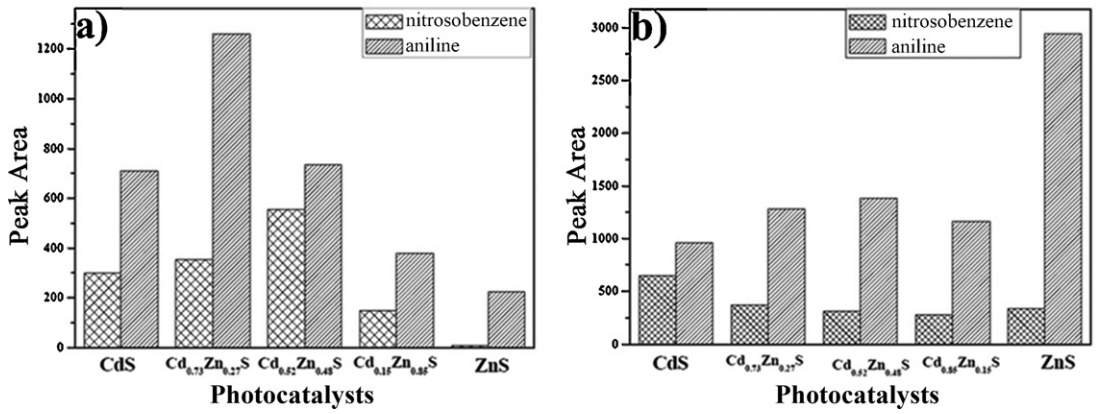

Fig. 6. Photocatalytic reduction of nitrobenzene over $Cd_xZn_{(1-x)}S$ solid solution under visible (a) and UV-light (b) irradiation.

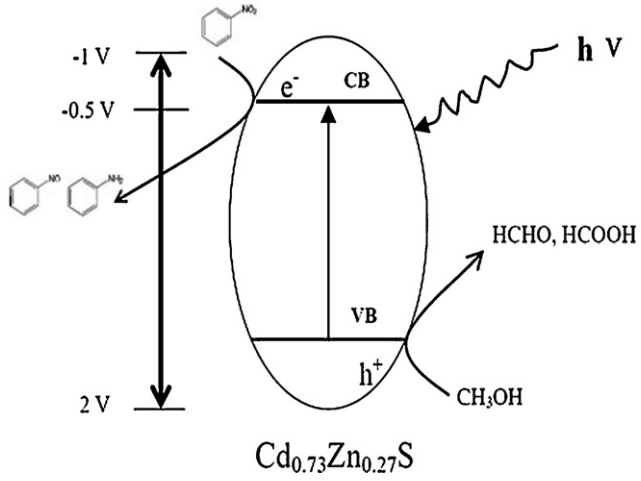

Fig. 7. Reaction mechanism of nitrobenzene reduction over $Cd_{0.73}Zn_{0.27}S$ sample.

recombination of photogenerated electron–hole pairs during the transfer process. The E_{CB} (−0.88 V vs. SCE) of $Cd_{0.73}Zn_{0.27}S$ is more negative than the reduction potential of nitrobenzene (−0.5 V vs. SCE) [49], which is beneficial to the reduction of nitrobenzene. Owing to these factors, $Cd_{0.73}Zn_{0.27}S$ exhibits the highest activity under visible-light irradiation. The reaction mechanism was shown in Fig. 7. When irradiated with UV light, ZnS sample exhibited the highest activity due to its negative conduction band, high surface area, and thin belt-like microstructure.

The photocatalytic reduction of NB over $Cd_xZn_{(1-x)}S$ semiconductor alloys is discussed as follows: (1) Production of photogenerated hole–electron pairs. When irradiated by photos with energy equal or larger than its band gap, electrons transfer from the valence band of $Cd_xZn_{(1-x)}S$ to conduction band, producing oxidative photogenerated valence holes (h^+) and reductive conduction electrons (e^-) (Eq. (4)). (2) Photogenerated holes and electrons without recombination move to $Cd_xZn_{(1-x)}S$ photocatalyst's surface. (3) Chemical reactions between photogenerated carriers and adsorbents. The holes are captured by CH_3OH solvent, producing HCHO oxide and reductive $H^\bullet$ (Eqs. (5) and (6)). NB is reduced by photogenerated electrons and $H^\bullet$, producing nitrosobenzene and aniline further [50] (Eq. (7)).

$$Cd_xZn_{(1-x)}S + h\nu \rightarrow Cd_xZn_{(1-x)}S(h^+ + e^-) \quad (4)$$

$$CH_3OH + h^+ \rightarrow CH_3O^\bullet + {}^\bullet CH_2OH \quad (5)$$

$$CH_3O^\bullet + {}^\bullet CH_2OH \rightarrow 2HCHO + 2H^\bullet \quad (6)$$

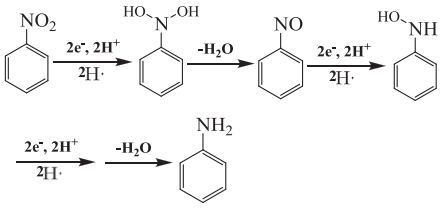

(7)

4. Conclusion

In summary, a series of hexagonal-phased $Cd_xZn_{(1-x)}S$ semiconductor alloys with tuneable band gaps were successfully prepared in a mixed solvent of ethylenediamine and water (v/v) at 180 °C for 12 h. Results showed that the products' microstructures, BET specific areas, UV–vis absorption spectral changed gradually with the increase of Zn content. Photocatalytic production of aniline via nitrobenzene reduction from CH_3OH as a solvent in the absence of oxygen was investigated. $Cd_{0.73}Zn_{0.27}S$ exhibited the highest activity under visible-light irradiation due to its energy band structures, large specific areas, and one-dimensional nanobelt-like microstructures.

Acknowledgment

We express our thanks to financial support from National Natural Science Fund of China (NSFC 50972083, 21071124 and 21173189).

References

[1] A. Fujishima, K. Honda, Nature 238 (1972) 37.
[2] W.Y. Choi, A. Termin, M.R. Hoffmann, J. Phys. Chem. 84 (1994) 13669.
[3] S.U.M. Khan, M. Al-Shahry, W.B. Ingler Jr., Science 297 (2002) 2243.
[4] S. Sakthivel, M. Janczarek, H. Kisch, J. Phys. Chem. B 108 (2004) 19384.
[5] X. Du, J.H. He, Y.Q. Zhao, J. Phys. Chem. C 113 (2009) 14151.
[6] Y. Matsumoto, M. Murakami, T. Shono, T. Hasegawa, T. Fukumura, Science 291 (2001) 854.
[7] S.Q. Peng, R. An, Y.X. Li, G.X. Lu, S.B. Li, Hydrogen Energy 37 (2012) 1366.
[8] Y.X. Li, D. Gao, S.Q. Peng, G.X. Li, S.B. Li, Int. J. Hydrogen Energy 36 (2011) 4291.
[9] H.W. Gu, R.K. Zheng, X.X. Zhang, B. Xu, J. Am. Chem. Soc. 126 (2004) 5664.
[10] K.W. Kwon, M. Shim, J. Am. Chem. Soc. 127 (2005) 10269.
[11] A. Zaban, O.I. Mićić, B.A. Gregg, A.J. Nozik, Langmuir 14 (1998) 3153.
[12] Y.H. Zheng, L.R. Zheng, Y.Y. Zhan, X.Y. Lin, Q. Zheng, K.M. Wei, Inorg. Chem. 46 (2007) 6980.
[13] G.K. Mor, K. Shankar, M. Paulose, O.K. Varghese, C.A. Grimes, Nano Lett. 6 (2006) 215.
[14] G.J. Meyer, Inorg. Chem. 44 (2005) 6852.
[15] Y.X. Li, G.F. Ma, S.Q. Peng, G.X. Lu, S.B. Li, Appl. Catal. A 363 (2009) 180.
[16] G.Z. Shen, D. Chen, C.J. Lee, J. Phys. Chem. B 110 (2006) 15689.
[17] X. Zong, H.J. Yan, G.P. Wu, G.J. Ma, F.Y. Wen, L. Wang, C. Li, J. Am. Chem. Soc. 130 (2008) 7176.
[18] J.Y. Kim, F.E. Osterloh, J. Am. Chem. Soc. 127 (2005) 10152.
[19] S.J. Park, Y.S. Jang, J.W. Shim, S.K. Ryu, J. Colloid Interface Sci. 260 (2003) 259.
[20] K. Zhang, D.W. Jing, C.J. Xing, L.J. Guo, Int. J. Hydrogen Energy 32 (2007) 4685.
[21] C.J. Xing, Y.J. Zhang, W. Yan, L.J. Guo, Int. J. Hydrogen Energy 31 (2006) 2018.
[22] W.J. Li, D.Z. Li, W.J. Zhang, Y. Hu, Y.H. He, X.Z. Fu, J. Phys. Chem. C 114 (2010) 2154.
[23] S.G. Zu, Z.Y. Wang, B. Liu, X.P. Fan, G.D. Qian, J. Alloys Compd. 476 (2009) 689.
[24] S. Guha, B.J. Wu, H. Cheng, J.M. Depuydt, Appl. Phys. Lett. 63 (1993) 2129.
[25] Y. Wada, D. Niinobe, M. Kaneko, Y. Tsukahara, J. Alloys Compd. 35 (2006) 62.
[26] Y.K. Liu, J.A. Zapien, Y.Y. Shan, C. Geng, C.S. Lee, S. Lee, Adv. Mater. 17 (2005) 1372.
[27] T. Zhai, Z. Gu, W. Yang, X. Zhang, J. Huang, Y. Zhao, D. Yu, H. Fu, Y. Ma, J. Yao, Nanotechnology 17 (2006) 4644.
[28] Z.Y. Yang, P. Zhang, W. Zhong, Y. Deng, C.T. Au, Y.W. Du, CrystEngComm 14 (2012) 4298.
[29] T.Y. Zhai, X.Z. Zhang, W.S. Yang, Y. Ma, J.F. Wang, Z.J. Gu, D.P. Yu, H. Yang, J.N. Yao, Chem. Phys. Lett. 427 (2006) 371.
[30] Y.F. Yu, J. Zhang, X. Wu, W.W. Zhao, B. Zhang, Angew. Chem. Int. Ed. 50 (2011) 1.
[31] H. Tada, T. Ishida, A. Takao, S. Ito, Langmuir 20 (2004) 7898.
[32] O. Makarova, T. Rajh, M. Thurnauer, Environ. Sci. Technol. 34 (2000) 4797.
[33] T.K. Kima, M.N. Leea, S.H. Leeb, Y.C. Parkb, C.K. Jungb, J.H. Boo, Thin Solid Films 475 (2005) 171.
[34] I. Tsuji, H. Kato, H. Kobayashi, A. Kudo, J. Am. Chem. Soc. 126 (2004) 13406.
[35] P. Yan, Y. Xie, Y.T. Qian, X.M. Liu, Chem. Commun. 14 (1999) 1293.
[36] G.D. Moon, S. Ko, Y.N. Xia, U. Jeong, ACS Nano 4 (2010) 2307.
[37] J.W. Tang, Z.G. Zou, J.H. Ye, J. Phys. Chem. C 111 (2007) 12779.
[38] L. Wang, W.Z. Wang, M. Shang, W.Z. Yin, S.M. Sun, L. Zhang, Int. J. Hydrogen Energy 35 (2010) 19.
[39] Y.X. Li, Y.F. Hu, S.Q. Peng, G.X. Lu, S.B. Li, J. Phys. Chem. C 113 (2009) 9352.
[40] Y.P. Zhang, W. Liu, R.M. Wang, Nanoscale 4 (2012) 2394.
[41] S.L. Xiong, J.M. Shen, Q. Xie, Y.Q. Gao, Q. Tang, Y.T. Qian, Adv. Funct. Mater. 15 (2005) 1787.
[42] Z.H. Jing, J.H. Zhan, Adv. Mater. 20 (2008) 4547.
[43] K. Krishsas, R. Plane, Inorg. Chem. 5 (1966) 852.
[44] J. Yang, J.H. Zeng, S.H. Yu, L. Yang, G.E. Zhou, Y.T. Qian, Chem. Mater. 12 (2000) 3259.
[45] Z.X. Deng, C. Wang, X.M. Sun, Y.D. Li, Inorg. Chem. 41 (2002) 869.
[46] Y.C. Zhang, W.W. Chen, X.Y. Hu, Cryst. Growth Des. 7 (2007) 580.
[47] G. Palmisano, V. Augugliaro, M. Pagliaro, L. Palmisano, Chem. Commun. 33 (2007) 3425.
[48] A.L. Stroyuk, I.V. Sobran, A.V. Korzhak, A.E. Raevskaya, S.Y. Kuchmiy, Colloid Polym. Sci. 286 (2008) 489.
[49] S.O. Flores, O.R. Bernij, M.A. Valenzuela, I. Córdova, R. Gómez, R. Gutiérrez, Top. Catal. 44 (2007) 507.
[50] J.L. Ferry, W.H. Glaze, Langmuir 14 (1998) 3551.